Received 26 April 2016; | Revised 6 June 2016; | Accepted 6 June 2016

DOI: xxx/xxxx

ARTICLE TYPE

On the use of surfaces of section in the N-body ring problem

Juan F. Navarro | M.C. Martínez–Belda

[1]Dept. Matemática Aplicada, Universidad de Alicante, Alicante, Spain

Correspondence
*Juan F. Navarro, Dept. Matemática Aplicada, Universidad de Alicante. Email: jf.navarro@ua.es

Present Address
Carretera San Vicente del Raspeig s/n, 03690, San Vicente del Raspeig, Alicante

Summary

In the N-body ring problem, we investigate the motion of a massless body interacting with N bodies of equal masses at the vertices of a regular polygon that rotates around a central mass. In this paper, we analyze the use of different surfaces of section in the numerical exploration of the escape in the N-body ring problem, in order to get some conclusions about the geometry of the basins of escape in the corresponding configuration spaces.

KEYWORDS:
N-body ring problem, surface of section, escape, Celestial Mechanics

1 | INTRODUCTION

In 1859, Maxwell proposed a model to understand the stability of Saturn's rings[16], which was awarded the Adams Prize of the University of Cambridge in 1856. Furthermore, his model was corroborated by the NASA Cassini probe to Saturn in 2004. Maxwell concluded that each ring have to be made up of a very large number of small "unconnected" particles uniformly distributed at the vertices of a regular polygon rotating around a massive body at the center. He proved, by means of Fourier analysis and dispersion relations, that the relative equilibrium formed by an n-gon of small equal masses in orbit around a single large mass is stable. Since then, a great number of scientists have addressed this problem. For instance, it is remarkable the study of Tisserand in 1889[23], who reformulated Maxwell's analysis in an efficient manner, deriving a bound for the relation between the mass of each particle in the ring and the number of them in order the system be linearly stable.

In the last three decades, there has been an increasing attention of the scientific community to the N-body problem due to the discovery of rings around all the gas giant planets in the Solar System, but also to the fact that this configuration models some dynamical systems like planetary rings, asteroid belts, planets around a star, some kind of stellar formations and planetary nebula, to cite some examples.[4,13,14]

On the other hand, the escapes of a particle from a dynamical system is another subject that has attracted much interest in the last decades.[1,2,3,5,6,7,8,9,10,11,17,22,24,25] When the energy of a particle is larger than the energy of escape, the curve of zero velocity of the system opens and many particles escape from the potential well. However, there are regions of orbits that never escape, or escape after a very long time. For each value of the energy larger than the energy of escape, there is a highly unstable periodic orbit at every opening of the curve of zero velocity. These periodic orbits are called Lyapunov orbits. The stable and unstable manifolds to these orbits form impenetrable boundaries in the phase space, and the projection of these manifolds from the phase space into the position space confines the domain of initial conditions of the escaping orbits.

The use of surfaces of section has been proved to be a powerful method to perform a numerical study of many problems in celestial mechanics and stellar dynamics. This technique dates back to Poincaré[21] and consists essentially in considering not a complete trajectory in the plane space but only its successive intersections with a certain surface of section. In 2019, Navarro and Martínez–Belda[20] started a numerical study of the escape in the N-body ring problem by using a surface of section defined by the hyperplane $y = 0$. The aim of this work is to consider a different surface of section which fits better to the symmetry of the problem, in order to understand some aspects about the geometry of the escape of a particle from the N-body ring configuration.

For each surface of section analyzed, we define a grid of initial conditions regularly distributed in the area allowed by the value of the energy. Then, we integrate numerically these initial conditions over $T = 10^2$ time units as a maximum time of numerical integration, to determine if the orbit escapes from the potential well or not. We have chosen $T = 10^2$ as maximum time of integration because our interest is focused in the analysis of the information obtained by considering a certain surface of section in the study of the escape of a particle from the potential well in the N-body ring configuration, and this analysis can be easily performed by taking short times of integration.

2 | EQUATIONS OF MOTION

Let us recall briefly the equations of motion of the N-body ring problem. The scenario considered in the ring configuration consists of a central body P_0, with mass m_0, located at the center of mass of the system, and N small bodies of equal masses, m, arranged at equal distances among them on the periphery of a circle.[15] These massive bodies are usually named "primaries". The subject of interest is the motion of a particle S of negligible mass moving under the resultant gravitational action of this system.

We assume that the peripheral bodies rotate at constant angular velocity, here taken as unity, and consider a synodic coordinate system $Oxyz$, with origin O at the center of mass of the system.[13,14] Assuming that the side of the regular polygon inscribed in the circle has a unit value, the equations that describe the planar motion of the small body S can be written as

$$\ddot{x} = 2\dot{y} + \frac{\partial U}{\partial x}\,, \quad \ddot{y} = -2\dot{x} + \frac{\partial U}{\partial y}\,. \tag{1}$$

The system is autonomous and there is a Jacobian-type integral of motion, which is given by

$$C = 2U(x, y) - (\dot{x}^2 + \dot{y}^2)\,, \tag{2}$$

where C is the Jacobian constant, and

$$U(x, y) = \frac{1}{2}(x^2 + y^2) + \frac{1}{\Delta}\left(\frac{\beta}{r_0} + \sum_{\nu=1}^{N}\frac{1}{r_\nu}\right).$$

The parameter $\beta = m_0/m$ is the ratio of the central mass to each peripheral one,

$$r_0 = \sqrt{x^2 + y^2}$$

is the distance from the central body to the test particle, and

$$r_\nu = \sqrt{(x - x_\nu^*)^2 + (y - y_\nu^*)^2}\,,$$

for $\nu = 1, 2, \ldots, N$, are the distances of the particle from the peripheral primaries. The variables x_ν^* and y_ν^* are the coordinates of the peripheral primaries,

$$x_\nu^* = \frac{1}{2\sin\theta}\cos(2(\nu - 1)\theta)\,, \quad y_\nu^* = \frac{1}{2\sin\theta}\sin(2(\nu - 1)\theta)\,,$$

and Δ is given by

$$\Delta = M(\Lambda + \beta M^2)\,,$$

where

$$\Lambda = \sum_{\nu=2}^{N}\frac{\sin^2\theta\cos((N/2 + 1 - \nu)\theta)}{\sin^2((N + 1 - \nu)\theta)} = \sum_{\nu=2}^{N}\frac{\sin^2\theta}{\sin((\nu - 1)\theta)}\,,$$

and

$$M = \sqrt{2(1 - \cos\psi)} = 2\sin\theta\,.$$

Finally, ψ is the angle between the central and two succesive peripheral primaries, and $\theta = \psi/2 = \pi/N$.

The curves of zero velocity can be obtained through

$$C = 2U(x, y) = x^2 + y^2 + \frac{2}{\Delta}\left(\frac{\beta}{r_0} + \sum_{\nu=1}^{N}\frac{1}{r_\nu}\right). \tag{3}$$

These curves form the boundaries that the test particle can not cross. In Figure 1 , we show the curves of zero velocity for $N = 5$, $\beta = 2$ and several values of the Jacobi constant C.

There is a critical value of the Jacobi constant, denoted by C_e, such that, for smaller values of C, the potential well is open and extends to infinity and then test particles may escape. Due to the symmetries of the potential, the well opens up at N places

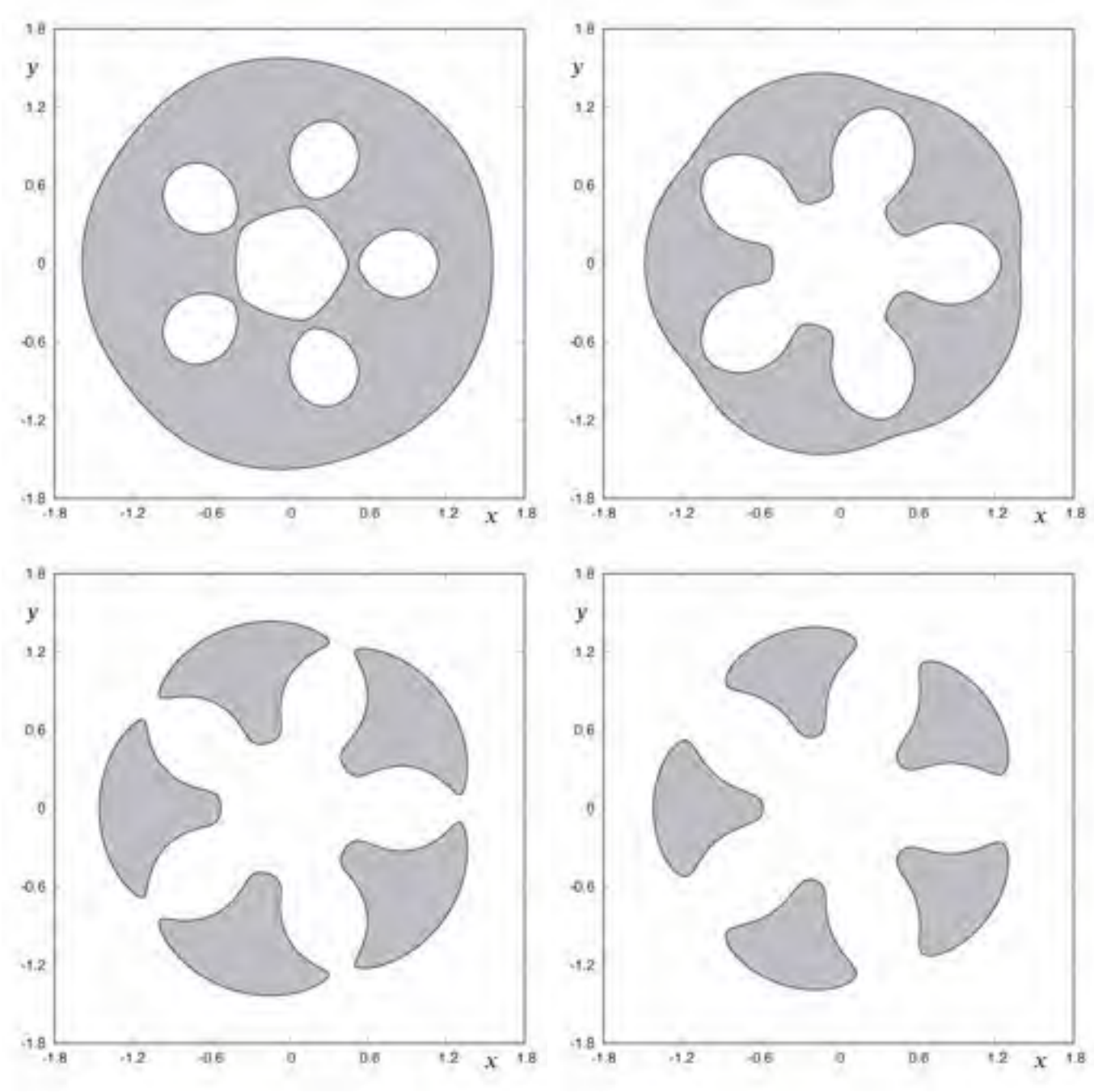

FIGURE 1 Curves of zero velocity for $N = 5$, $\beta = 2$ and $C = 4.2$ (upper-left panel), $C = 4$ (upper-right panel), $C = 3.96$ (lower-left panel) and $C = 3.9$ (lower-right panel). We show in grey the regions where the particle motion is impossible to happen.

in the configuration space (see Figure 2). For each value of C smaller than C_e, there is a highly unstable periodic orbit that bridges the minimum openings of the curve of zero velocity, bouncing back and forth between the two walls of the pass. Such orbits are called “Lyapunov orbits" and they are always unstable. Their most important property is that any orbit crossing them outwards moves always outwards and escapes from the system. These orbits intersect perpendicularly the lines defined by

$$y = \tan(2(\nu - 1)\theta)x\,, \quad \theta = \frac{\pi}{N}\,,$$

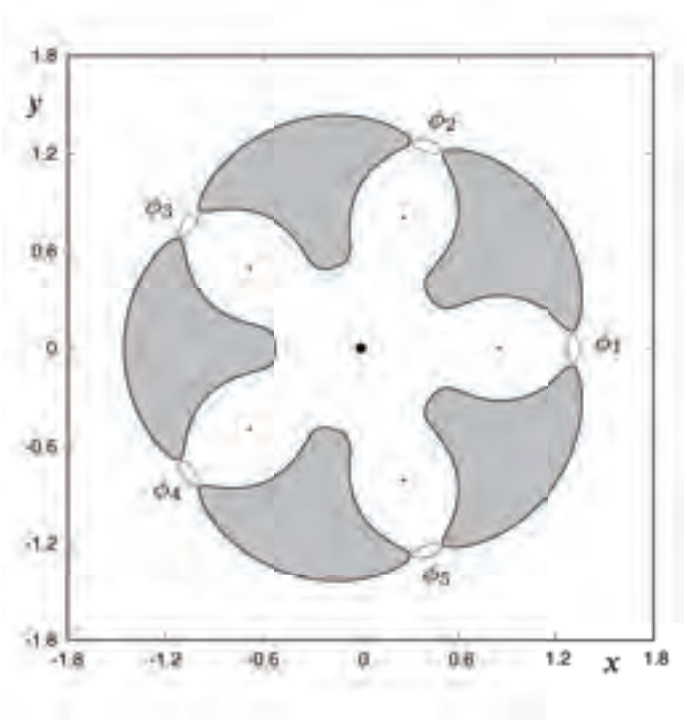

FIGURE 2 Curves of zero velocity for $N = 5$, $\beta = 2$ and $C = 3.96$. There is a highly unstable periodic orbit at every opening of the curve of zero velocity.

for $\nu = 1, \ldots, N$. We have numbered the openings of the potential well, as well as the associated Lyapunov orbits (ϕ_ν, $\nu = 1, \ldots, 5$) as detailed in Figure 2 . Inside the region defined by the Lyapunov orbits, there are sets of orbits that escape, and sets of orbits which remain trapped.

In Figure 2 , we show the curves of zero velocity for $N = 5$, $\beta = 2$ and $C = 3.96$. The value of C_e for $N = 5$ and $\beta = 2$ is given by $C_e = 3.971595480$. In our computations, we have performed the numerical integration over $T = 10^2$ time units as a maximum time of numerical integration, to test each surface of section and analyze the basins of escape of the test particle. The escape time $t_{\rm esc}$ is defined as the time a particle needs to cross one of the Lyapunov orbits with velocity pointing outwards. Orbits that do not escape after a numerical integration of 10^4 time units are considered as non-escaping or trapped orbits. Our numerical calculations indicate that the percentage of escaping orbits do not vary significantly by considering a maximum time of integration T of 10^3 or 10^4. Whereas for a maximum integration time of 10^2 units only 21.3% of orbits escape from the potential well, for $T = 10^3$ and 10^4, the percentages of escaping orbits are 52.03% and 52.75%, respectively.[20] However, we have chosen $T = 10^2$ as the maximum time of integration because our interest is focused on the analysis of the advantages and disadvantages of considering a certain surface of section to study the escape of a particle from the potential well in the N-body ring configuration, and this analysis can be performed in a clearer way by considering short times of integration.

We have used the RPS method for the numerical integration.[18,19] The precision of the method has been fixed to $\epsilon = 10^{-23}$, and the number of term series to 26. With these parameters, the Jacobi constant C of the equations of motion remains the same to 17 significant figures along the numerical integration of the problem.

3 | FIRST SURFACE OF SECTION

In order to explore the escape dynamics of a test particle in the N-body ring problem, we need to define a grid of initial conditions regularly distributed in the area allowed by the value of the energy. We start our investigation in the $(x, \dot{x})$ space, taking as surface of section the hyperplane $y = 0$. Thus, we consider orbits with initial conditions $(x_0, \dot{x}_0)$ with $y_0 = 0$, while the initial

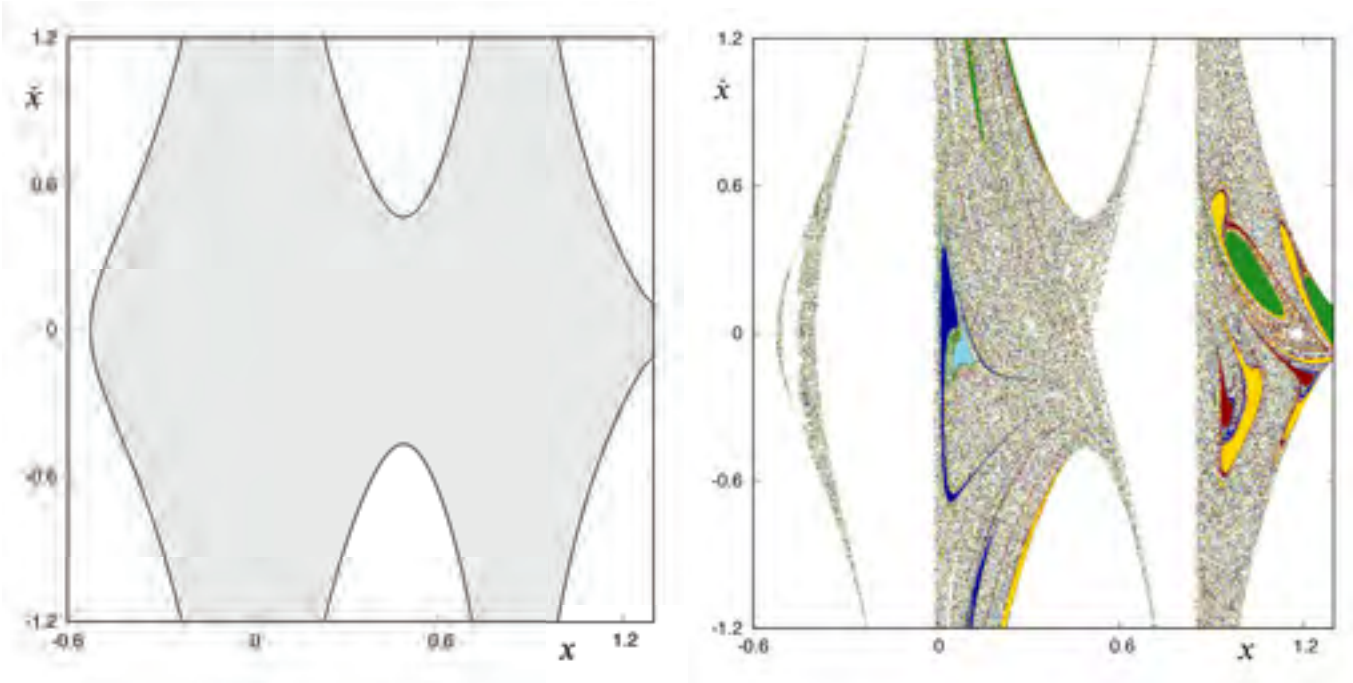

FIGURE 3 Domain D_1 of allowed initial conditions on the phase $(x, \dot{x})$, for $N = 5$ and $C = 3.96$ (left panel). Structure of the phase $(x, \dot{x})$ for $N = 5$, $C = 3.96$, and a maximum time of integration of $T = 10^2$ (right panel).

value of $\dot{y}_0$ is obtained through the equation

$$\dot{y}_0 = +\sqrt{2U(x_0, 0) - C - \dot{x}_0^2}\,.$$

This implies that the initial conditions must be taken in the domain D_1 defined by

$$D_1 = \{(x_0, \dot{x}_0) \in \mathbb{R}^2 \ : \ 2U(x_0, 0) - \dot{x}_0^2 \geq C\}\,.$$

In Figure 3 (left panel), we represent (in grey) this domain.

The initial conditions on the surface of section $(x, \dot{x})$ that lead to escapes through the various Lyapunov orbits form the corresponding basins of escape. In Figure 3 (right panel), we show the basins of escape considering a maximum time of numerical integration of $T = 10^2$, for the value of the Jacobi constant $C = 3.96$. We have used different colors in order to distinguish between the five channels of escape, and initial conditions leading to collisions (black). Initial conditions colored in green correspond to orbits leaving the potential well through the opening 1. Initial conditions in light blue, dark blue, dark red and yellow correspond to orbits escaping through channels 2, 3, 4 and 5, respectively (see Figure 4). We observe large connected domains that lead to the same kind of escape, but also some regions where the different basins are intricately mixed. These regions have a very sensitive dependence of the escape process on the initial conditions. That means that a slight change in the initial conditions makes the particle escape through a different window. In these chaotic domains, the green, light blue, dark blue, dark red and yellow regions are completely intertwined with respect to each other: the boundary between these regions is fractal.

In the right panel of Figure 3 , we observe that the large connected domains leading to the same kind of escape are interrelated. In the domains located around values of x in the interval $(0, 0.3)$, we can distinguish two main connected structures: a primary structure colored in dark blue, and a secondary structure colored in light blue infinitely spiraling around the first one. These two structures correspond to initial conditions of orbits that escape through the exit windows guarded by the Lyapunov periodic orbits ϕ_3 and ϕ_2, respectively. We can also distinguish in this region some other tertiary and quaternary connected structures colored in dark red, yellow and green, but with smaller area.

On the other hand, for values of x in the interval $(0.9, 1.3)$, we find three main basins of escape in the connected domains: green, dark red and yellow, which are also interrelated, and correspond to initial conditions of orbits leaving the potential well through the exit windows guarded by the Lyapunov orbits ϕ_1, ϕ_4 and ϕ_5, respectively. This fact implies that there is no symmetry

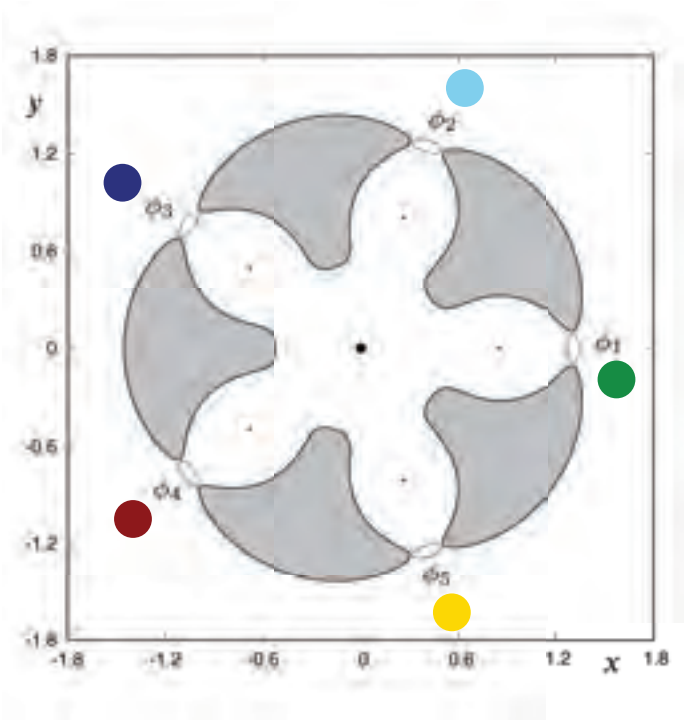

FIGURE 4 We have used different colors in order to distinguish between the five channels of escape. Initial conditions in green, light blue, dark blue, dark red and yellow correspond to orbits escaping through channels 1, 2, 3, 4 and 5, respectively.

with respect to the y axis. The main windows through which particles escape directly are those guarded by the periodic orbits ϕ_2 and ϕ_3. The stable manifolds of the unstable periodic orbits located at the minimum openings of the curve of zero velocity form the boundaries of the basins of escape and the shape of the unstable manifolds of the Lyapunov orbits is responsible for the ring and spiral structures found in the configuration space. This means that the connected domains that we observe in Figure 3 give us information about the location of the stable manifold to the corresponding guardian periodic orbit. It is clear that orbits with initial conditions inside the well-defined exit basins escape from the system very quickly, that is, they have remarkably small times of escape.

In Figure 3 , we also observe three main domains in white corresponding to initial conditions which remain trapped in the potential well. The choice of the hyperplane $y = 0$ has the advantage of providing information about the escape in the variables x and $\dot{x}$. On the other hand, it does not reflect the circular symmetry of the configuration.

4 | SECOND SURFACE OF SECTION

Now, we will consider a surface of section which is more suitable for the circular symmetry of the problem. Let us introduce polar coordinates (r, θ), i.e., $x = r\cos\theta$, $y = r\sin\theta$. Here, we define the surface of section $r = 0.3$, and consider the configuration space (θ, α), where $\theta \in [0, 2\pi]$ and $\alpha \in [0, 2\pi]$ are defined through the relations

$$x = r\cos\theta\,, \quad y = r\sin\theta\,,$$

and

$$\dot{x} = v\cos\alpha\,, \quad \dot{y} = v\sin\alpha\,,$$

being v the modulus of the velocity (see Figure 5 , left panel). We proceed as follows: first, for a given value of θ, we compute x and y and the modulus of the velocity through the relation

$$v^2 = \dot{x}^2 + \dot{y}^2 = 2U(x, y) - C\,.$$

Then, we set the value of the angle α of the velocity vector, and we compute $\dot{x}$ and $\dot{y}$.

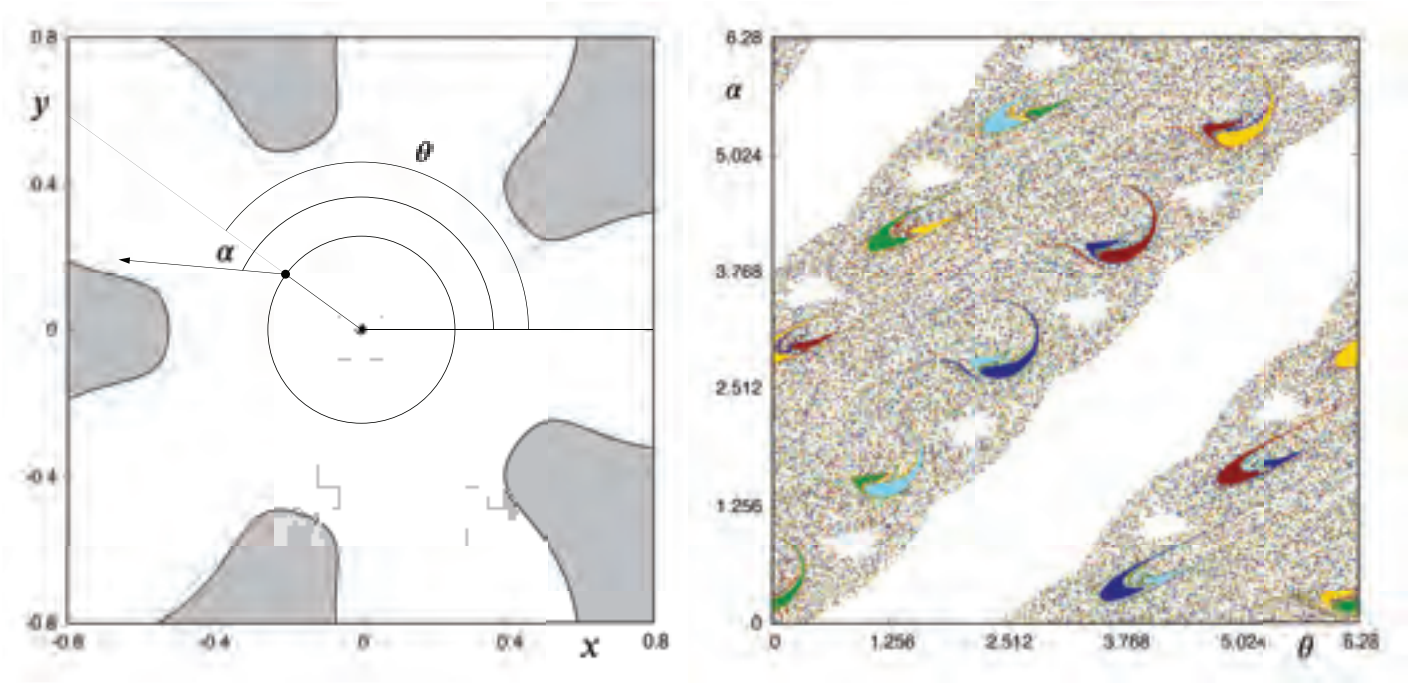

FIGURE 5 Structure of the phase (θ, α) for $N = 5$, $C = 3.96$, and a maximum time of integration of $T = 10^2$.

The initial conditions on the surface of section (θ, α) that lead to escapes through the various Lyapunov orbits form the corresponding basins of escape. In Figure 5 (right panel), we show the basins of escape considering a maximum time of numerical integration of $T = 10^2$, for the value of the Jacobi constant $C = 3.96$. As in the previous case, we have used different colors in order to distinguish between the five channels of escape, and initial conditions leading to collisions (Figure 4). We observe also in this case large connected domains, that lead to the same kind of escape. These domains compose a repeating pattern along the diagonal $\alpha = \theta$, which evidences how the projection of the stable and unstable manifolds to the guardian unstable periodic orbits from the phase space into the (θ, α) space organize the geometry of the basins of escape in this space.

Let us notice that there are five connected tongue shaped domains distributed along the diagonal $\alpha = \epsilon_1 + \theta$, where $\epsilon_1 \simeq \pi/20$, and centered at the values of θ given by $\theta = 2\pi(n-1)/5$ (and $\alpha = \epsilon_1 + 2\pi(n-1)/5$), for $n = 1, 2, 3, 4, 5$. These values of the angles correspond to orbits with initial conditions approximately pointing to the location of the primaries. We can also identify a secondary tongue surrounding the main tongue. The color of this secondary tongue corresponds to initial conditions of orbits escaping through the previous window of the potential well. That is, for $n = 2$, we find a main tongue colored in light blue (second exit window), and a secondary tongue colored in green surrounding it (first exit window). For $n = 3$, the main tongue is colored in dark blue (third exit window) and the secondary tongue surrounding it is colored in light blue (second exit window).

In Figure 6 , we show the representation of an initial condition (θ_0, α_0) in the (x, y) plane (left panel), belonging to the main tongue of the structure located along the main diagonal $\alpha = \epsilon_1 + \theta$, for $\theta = 2\pi(n-1)/5$ and $n = 3$. In the right panel of Figure 6 , we indicate (symbol $\star$) the location of the initial condition in the (θ, α) space. There, we can observe that the basins of escape of the orbits with initial conditions located around $\alpha = \epsilon_1 + \theta$, for values of θ near $4\pi/5$ have the following composition: a big tongue-shaped domain in dark blue, and a secondary domain in light blue infinitely spiraling around the first tongue. But there are also a third structure colored in green infinitely spiraling around these two tongues, a fourth structure in yellow and, finally, a fifth domain in dark red. All these five structures are closely interrelated. We can conclude that the magnitude of the area of these regions can be ordered following a clockwise tour along the exit windows in the configuration space (x, y), and starting from the exit channel guarded by ϕ_3, as indicated in the left panel of Figure 6 .

There is also a second structure composed by a pair of main tongues, which are interrelated and located along a secondary diagonal defined by $\alpha = \epsilon_2 + 4\pi/5 + \theta \pmod{2\pi}$, where $\epsilon_2 \simeq \pi/10$, and for the same values of θ that in the first structure, that is, $\theta = 2\pi(n-1)/5$ (and $\alpha = \epsilon_2 + 4\pi/5 + 2\pi(n-1)/5 \pmod{2\pi}$), for $n = 1, 2, 3, 4, 5$. These values of the angles correspond to orbits with initial conditions approximately pointing to the primary located at the opposite direction defined by the angle θ. As in the first structure described above, the color of the secondary tongue corresponds to initial conditions of orbits escaping

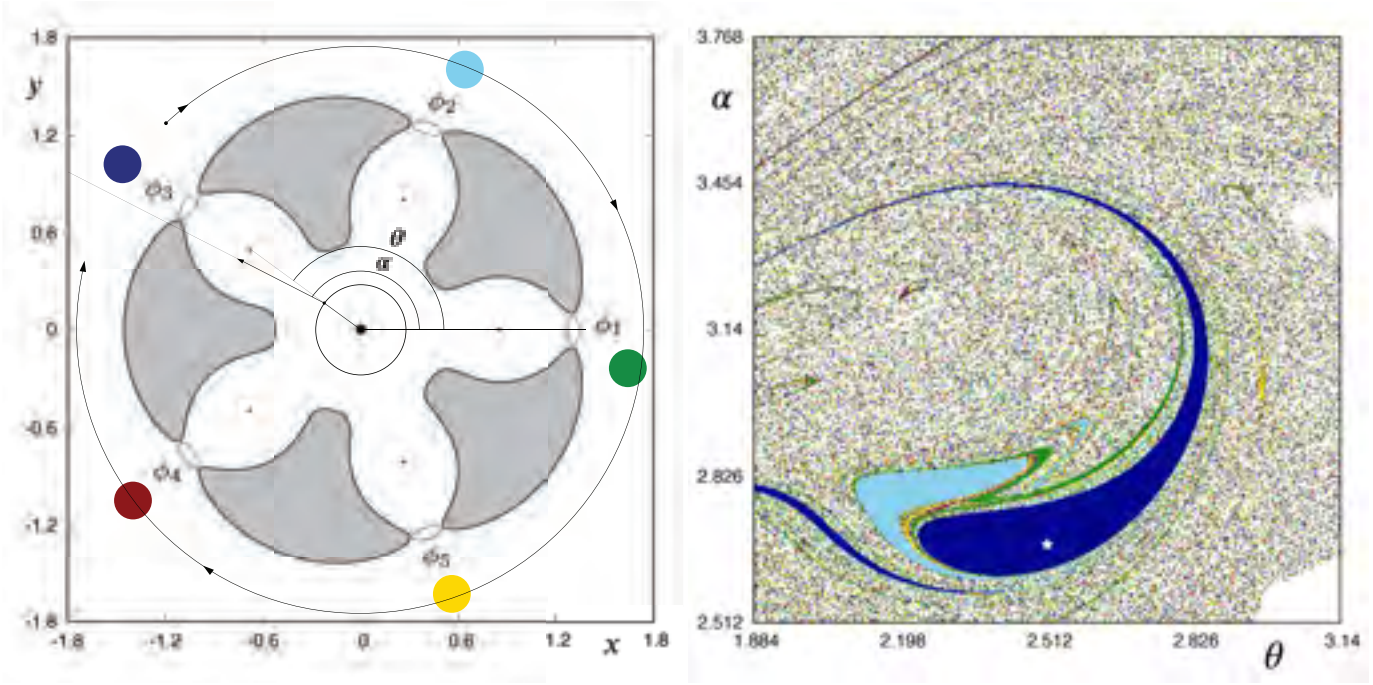

FIGURE 6 Second surface of section $r = 0.3$, and representation of an initial condition taken along the main diagonal: $\theta = 4\pi/5$ and $\alpha = 4\pi/5 + \pi/20$.

through the previous window of the potential well. That is, for $n = 2$, we find a main tongue colored in green (first exit window), and a secondary tongue colored in yellow surrounding it (fifth exit window). For $n = 3$, the main tongue is colored in light blue (second exit window) and the secondary tongue surrounding it is colored in green (first exit window).

In Figure 7 , we show the representation of an initial condition (θ_0, α_0) in the (x, y) plane (left panel), belonging to the main tongue of the structure located along the secondary diagonal $\alpha = \epsilon_2 + 4\pi/5 + \theta \pmod{2\pi}$, for $\theta = 2\pi(n-1)/5$ and $n = 3$. In the right panel of Figure 7 , we indicate (symbol $\star$) the location of the initial condition in the (θ, α) space. There, we can observe that the basins of escape of the orbits with initial conditions located around $\alpha = \epsilon_2 + 4\pi/5 + \theta \pmod{2\pi}$, and for values of θ near $4\pi/5$, have the following composition: a big domain in light blue, a secondary domain in green and, as in the previous case, a third structure colored in yellow infinitely spiraling around these two tongues, a fourth structure in dark red and, finally, a fifth domain in dark blue. All these five structures are closely interrelated. We can conclude that the magnitude of the area of these regions can be ordered following a clockwise tour along the exit windows in the configuration space (x, y), and starting from the exit channel guarded by ϕ_2, as indicated in the left panel of Figure 7 .

In Figure 8 , we show how the structures described in Figures 6 and 7 fill the configuration space (θ, α). These structures, related to the stable and unstable manifolds to the Lyapunov orbits located at the openings of the potential well, organize the geometry of the basins of escape in the configuration space (θ, α). In Figure 9 , we show a detail of a region of the configuration space (θ, α) to show clearly how this happens at any level of scale.

We have found also some regions where the different basins are intricately mixed. We find again a sensitive dependence of the escape process on the initial conditions, that is, slight changes in the initial condition of a particle cause an escape through a different window. In these chaotic domains, the green, light blue, dark blue, dark red and yellow regions are completely intertwined with respect to each other: the boundary between these regions is fractal. We have found that these fractal domains are bounded by the the projection of the stable and unstable manifolds to the guardian unstable periodic orbits from the phase space into the (θ, α) plane.

Now, we will analyze the distribution of the regions of initial conditions of trapped orbits. There are five domains in white along the main diagonal corresponding to initial conditions which remain trapped in the potential well. The centers of these white domains are located approximately at $\theta = \alpha = 8\pi/30 + 2\pi(n-1)/5$, for $n = 1, 2, 3, 4, 5$, that is, $4\pi/15, 2\pi/3, 16\pi/15, 22\pi/15, 28\pi/15$. In Figure 10 , we identify the location of these domains, marking their approximate

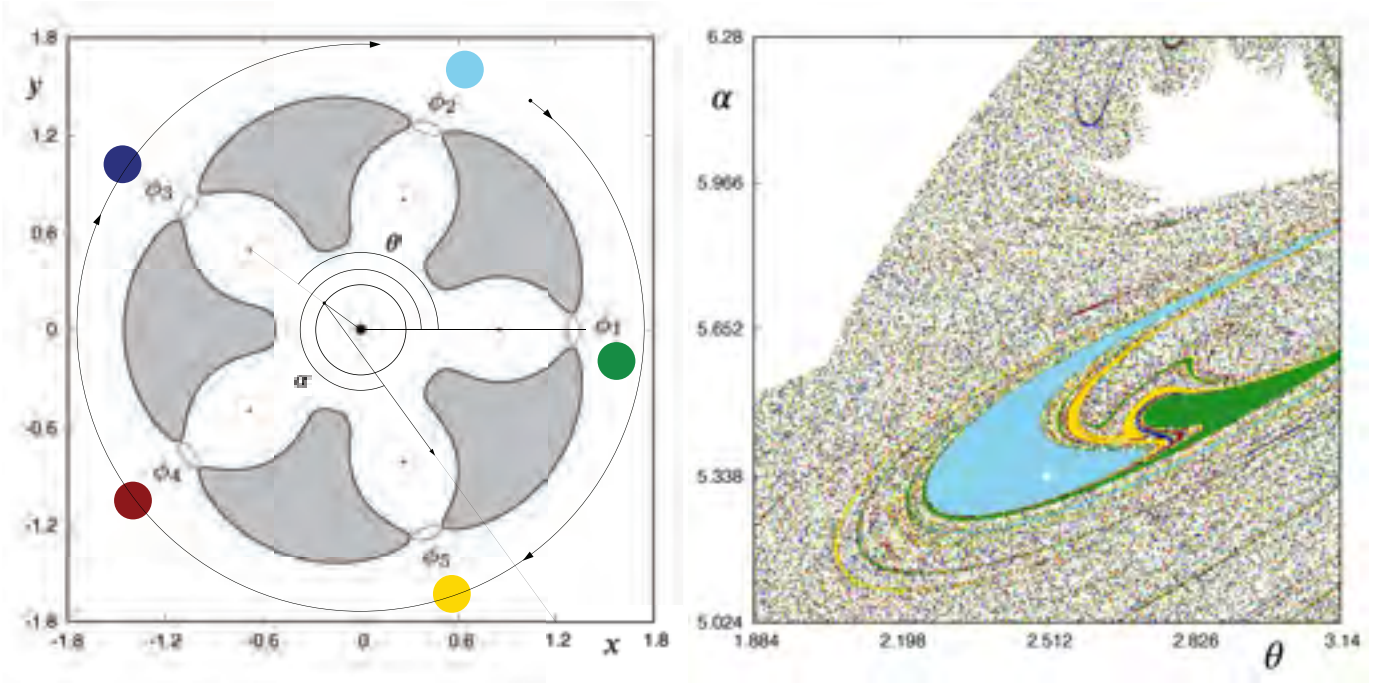

FIGURE 7 Second surface of section $r = 0.3$, and representation of an initial condition taken along the secondary diagonal: $\theta = 4\pi/5$ and $\alpha = 8\pi/5 + \pi/10$.

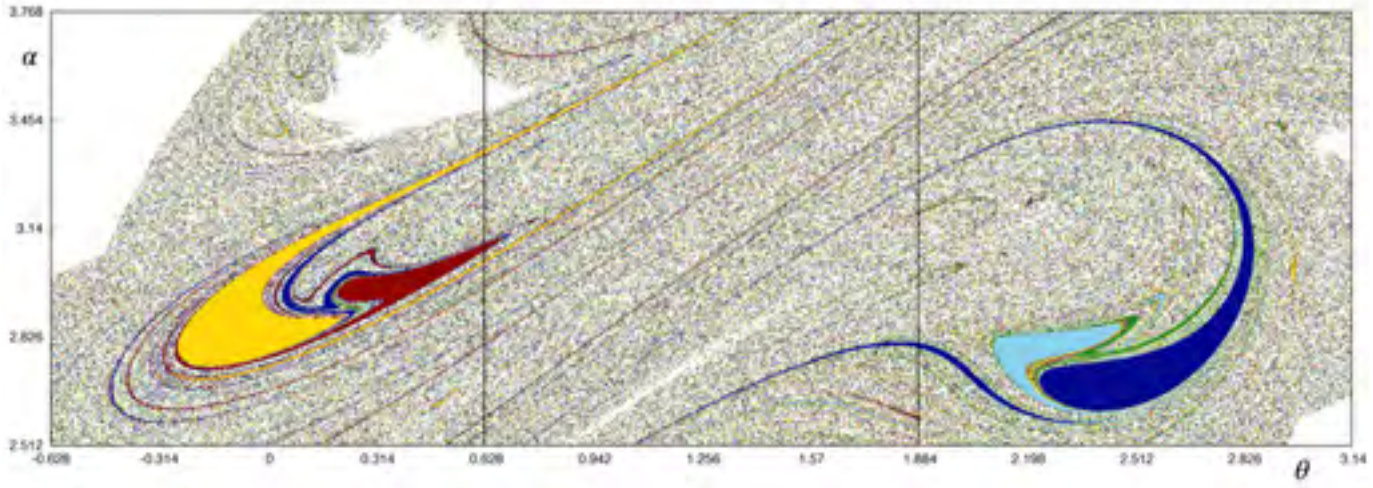

FIGURE 8 Detail of the structure of the phase (θ, α) for $N = 5$, $C = 3.96$, and a maximum time of integration of $T = 10^2$.

centers in the (θ, α) space (left panel). We also indicate in Figure 10 (right panel) the position and direction of the velocity of the initial conditions in the (x, y) configuration space.

There are also some other five domains in white along a secondary diagonal defined by $\alpha = \pi + \theta \pmod{2\pi}$, corresponding to initial conditions which remain trapped in the potential well. The centers of these white domains are located approximately at $\theta = 4\pi/30 + 2\pi(n-1)/5$, for $n = 1, 2, 3, 4, 5$, that is, $2\pi/15, 8\pi/15, 14\pi/15, 4\pi/3, 26\pi/15$. As $\alpha = \theta + \pi$, the position and velocity vectors of the particle located at the circumference $r = 0.3$ have opposite directions. In Figure 11 , we identify the location of these domains, marking their approximate centers in the (θ, α) plane (left panel). We also indicate in Figure 11 (right panel) the position and direction of the velocity of the initial conditions in the (x, y) configuration space.

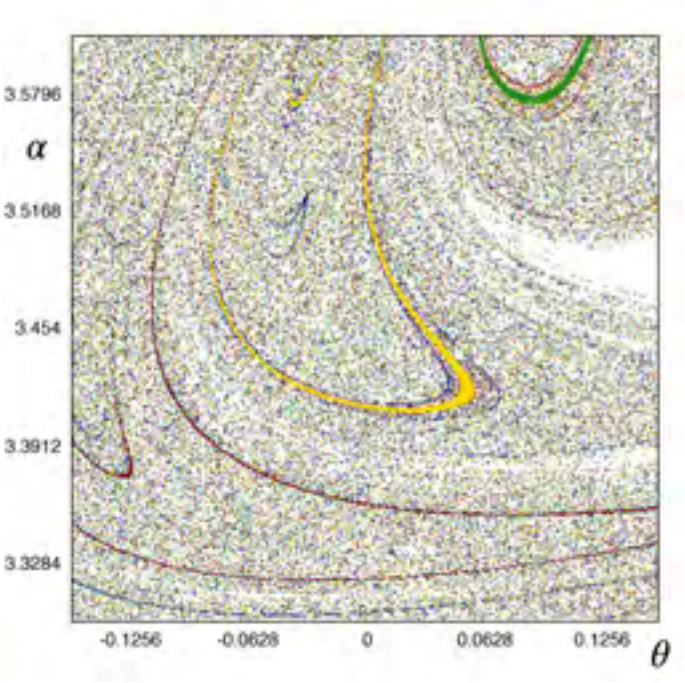

FIGURE 9 Detail of the structure of the phase (θ, α) for $N = 5$, $C = 3.96$, and a maximum time of integration of $T = 10^2$.

The main connected white domain corresponding to initial conditions of orbits remaining trapped in the potential well is a band approximately located between the lines defined by $\alpha = \theta + 8\pi/5 - \alpha_1 \pmod{2\pi}$ and $\alpha = \theta + 8\pi/5 + \alpha_2 \pmod{2\pi}$, where $\alpha_1 = 2\pi/5$ and $\alpha_2 = \pi/5$. In the left panel of Figure 12 , we identify the line $\alpha = \theta + 8\pi/5$, and the initial condition $\theta = 4\pi/5$, $\alpha = 2\pi/5$. We also indicate in Figure 12 (right panel) the position and direction of the velocity of this initial condition in the (x, y) configuration space.

Finally, there is still one aspect of the results we have obtained that should be analyzed. As we have taken a surface of section which is symmetric with respect to the location of the primaries, one may expect some symmetry in the basins of escape with respect to the $\alpha = \theta$ axes. However, if we consider initial conditions in the surface of section $r = 0.3$, with $\theta = (2n - 1)\pi/5$ (that is, located in the line joining the central mass and one of the primaries), and $\alpha = \theta + \epsilon$ and $\alpha = \theta - \epsilon$, respectively, the orbits related to these initial conditions do not evolve in the same way, as we can observe in Figure 5 . This asymmetry observed in the distribution of the connected regions with respect to the $\alpha = \theta$ axes must be due to the Coriolis forces. The direction of Coriolis forces is not perpendicular to the velocity of the particle.

5 | ANALYSIS IN THE (X, C) PLANE

In 1969, Hénon [12] introduced the section $y = \dot{x} = 0$, $\dot{y} > 0$ to study the restricted three-body problem. This plane has been also used by authors like Zotos [26], in his numerical exploration of the four-body problem, and Barrio and co-workers, in the analysis of the fractal structures in the Hénon–Heiles potential.[6] In this new plane, the initial conditions of the orbits are taken in the x axis, with $x = x_0$, $y = 0$, and with the initial velocity parallel to the y axis ($\dot{x} = 0$, $\dot{y} > 0$). Therefore, the value of the Jacobi constant C can be used as a parameter, and then we can study its influence in the orbital structure of the system.

In Figure 13 , we show the orbital structure of the (x, C) plane for values of the Jacobi constant in the interval $[3.6, 3.971]$. We have considered values of C smaller than the critical value C_e. The black solid line is the limiting curve which distinguishes between regions of allowed and forbidden motion (in light grey). This domain is defined by

$$D_2 = \{(x_0, C_0) \in \mathbb{R}^2 \ : \ 2U(x_0, 0) - C_0 \geq 0\} .$$

Figure 13 shows several large connected domains corresponding to initial conditions of orbits leading to the same kind of escape. A large portion of the (x, C) plane is covered by initial conditions of escaping orbits. As we have considered orbits with

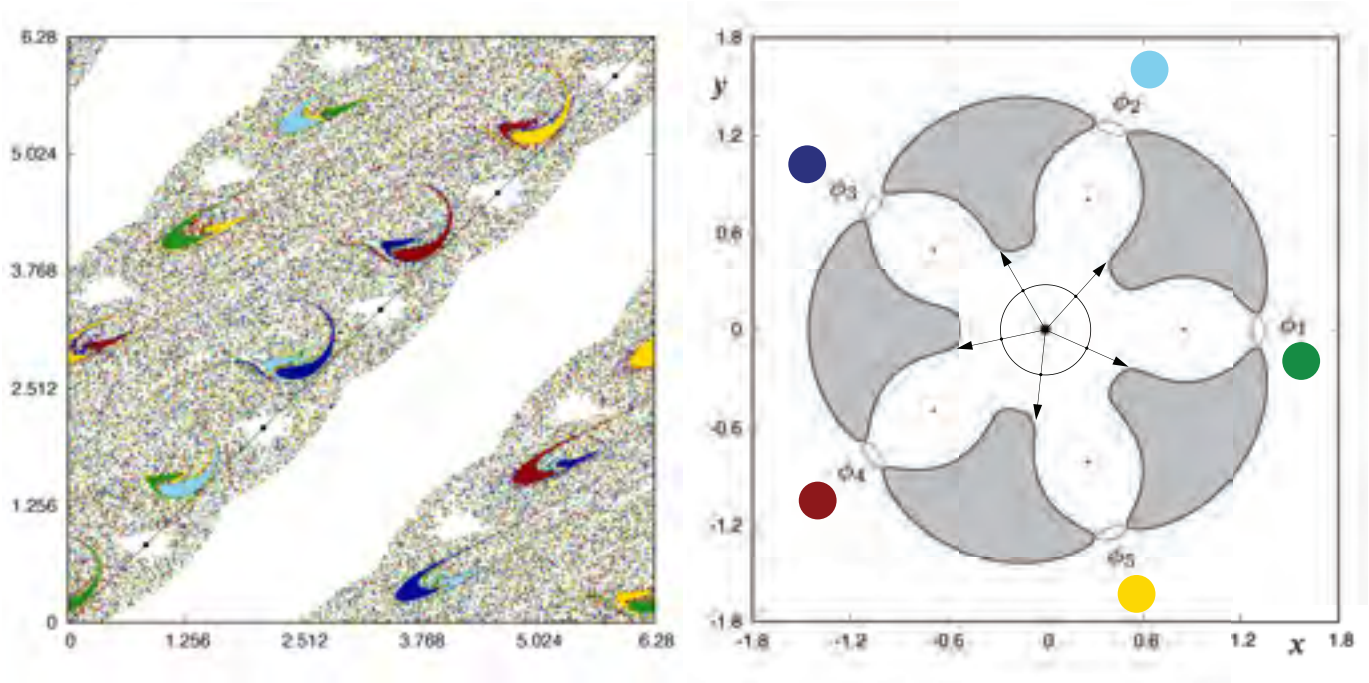

FIGURE 10 Representation of some initial conditions taken in the white regions along the main diagonal $\alpha = \theta$.

initial conditions along the x axis, with $\dot{x} = 0$ and $\dot{y} > 0$, we find a correlation between the value of the x coordinate associated to the location of the exit window and the color of the corresponding connected domain. We can also observe some regions where the different basins are intricately mixed. In these domains, there is a sensitive dependence of the escape process on the initial conditions. As the value of the Jacobi constant tends to the critical value $C_e = 3.971595480$, the chaotic area becomes larger. We also identify a pair of white bands, corresponding to initial conditions of orbits which remain trapped in the potential well. The first one is approximately located at values of x in the interval $(-0.6, 0)$ and is composed of initial conditions of orbits that circulate around the central body or one of the primaries. The second takes place for values of x in the interval $(0.55, 1)$.

6 | CONCLUSIONS

In this paper, we have explored some properties of the escape of a particle from the potential well of the N-body configuration through the analysis of two different surfaces of section. One of them has been extensively used in previous works, and the other, not used before, provides very useful information about the symmetry of the problem.

Conflict of interest

This work does not have any conflicts of interest.

References

1. Aguirre J, Vallejo JC, Sanjuan MAF. Wada basins and chaotic invariant sets in the Hénon–Heiles system. *Phys Rev E*. 2001;64:066208.
2. Aguirre J, Sanjuan MAF. Limit of small exits in open Hamiltonian systems. *Phys Rev E*. 2003;67:056201.
3. Aguirre J, Viana RL, Sanjuan MAF. Fractal structures in nonlinear dynamics. *Rev Mod Phys*. 2009;81:333-386.
4. Barrabés E, Cors JM, Hall GR. Numerical exploration of the limit ring problem. *Qual Theory Dyn Syst*. 2013;12:25-52.

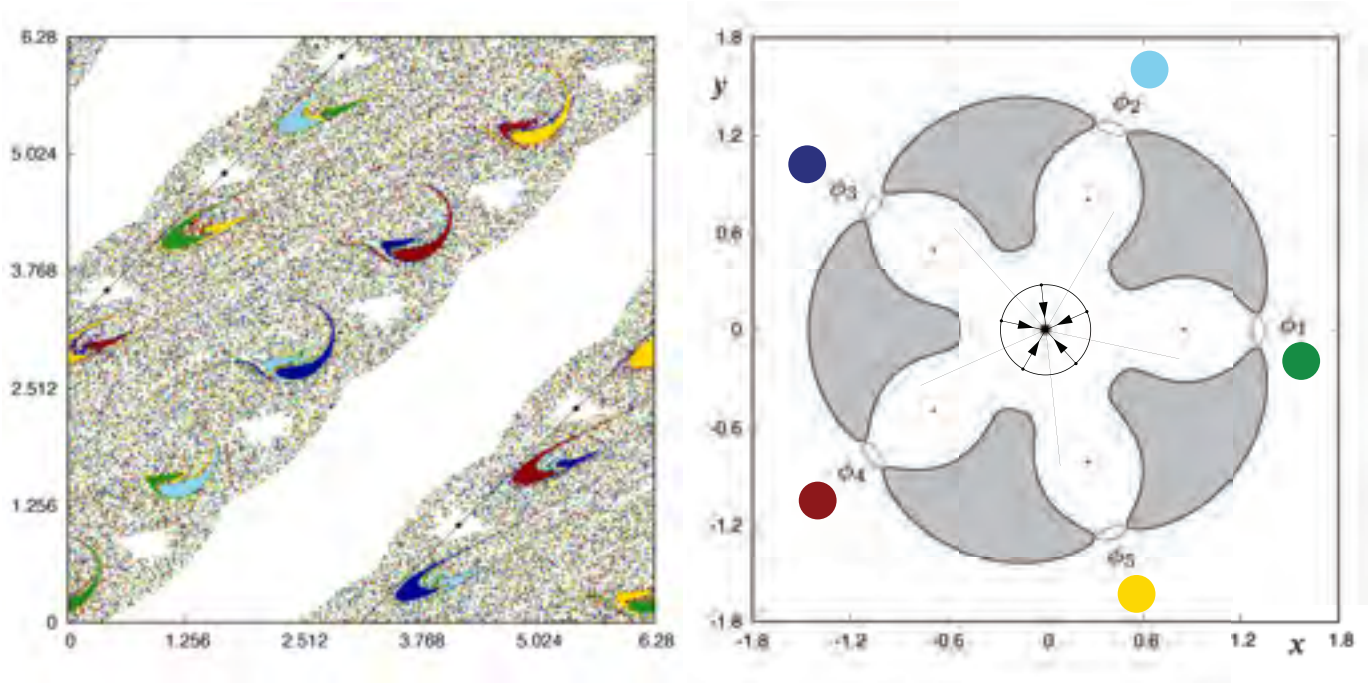

FIGURE 11 Representation of some initial conditions taken in the white regions along the secondary diagonal $\alpha = \pi + \theta$.

5. Barbanis B. Escape regions of a quartic potential. *Celest Mech Dyn Astron*. 1990;48(1):57-77.
6. Barrio R, Blesa F, Serrano S. Fractal structures in the Hénon–Heiles Hamiltonian. *Europhys Lett*. 2008;82:10003.
7. Barrio R, Blesa F, Serrano S. Bifurcations and safe regions in open Hamiltonians. *New Journal of Physics*. 2009;11:053004.
8. Barrio R, Blesa F, Serrano S. Bifurcations and chaos in Hamiltonian systems. *Int J Bifurcat Chaos*. 2010;20(5):1293-1319.
9. Contopoulos G. Asymptotic curves and escapes in Hamiltonian systems. *Astron Astrophys*. 1990;231(1):41-45.
10. Contopoulos G, Kaufmann D. Types of escapes in a simple Hamiltonian system, *Astron Astrophys*. 1992;253(2):379-388.
11. De Moura APS, Letelier PS. Fractal basins in Henon-Heiles and other polynomial potentials. *Phys Lett A*. 1999;256:362-368.
12. Hénon M. Numerical exploration of the restricted problem. *Astron Astrophys*. 1969;1:223-238.
13. Kalvouridis TJ. A planar case of the $n+1$ body problem: the 'ring' problem. *Astrophysics and Space Science*. 1999;260:309-325.
14. Kalvouridis TJ. Periodic solutions in the ring problem. *Astrophysics and Space Science*. 1999;266:467-494.
15. Kalvouridis TJ. On a property of zero–velocity curves in N-body ring–type systems. *Planetary and Space Science*. 2004;52:909-914.
16. Maxwell JC. *On the stability of motions of Saturn's rings*, Cambridge: Macmillan and Company; 1859.
17. Navarro JF, Henrard J. Spiral windows for escaping stars. *Astron Astrophys*. 2001;369:1112-1121.
18. Navarro JF. Numerical integration of the N-body ring problem by recurrent power series. *Celest Mech Dyn Astr*. 2018;130(2):16.
19. Navarro JF, Vargas J. On the long term numerical integration of a planetary ring. *J Comput Appl Math*. 2019;354:390-401.
20. Navarro JF, Martínez–Belda MC, Escaping orbits in the N-body ring problem, *Comp and Math Methods* (2019) accepted.

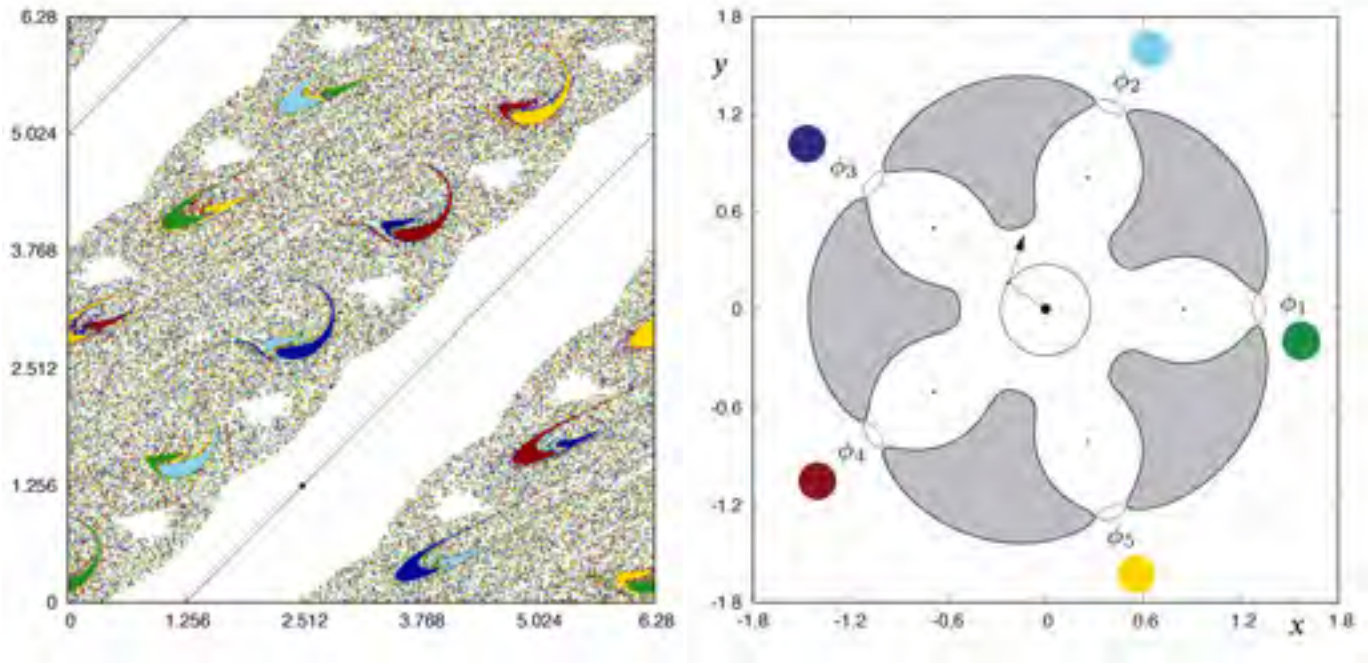

FIGURE 12 Representation of some initial conditions taken in the white regions along the main white domain around $\alpha = \theta + 8\pi/5$.

21. Poincaré H. *Les Methodes Nouvelles de la Mécanique Celeste I*. Paris: Gauthiers–Villars; 1892.

22. Siopsis C, Kandrup HE, Contopoulos G, Dvorak R. Universal properties of escape in dynamical systems. *Celest Mech Dyn Astron.* 1996;65(1-2):57-68.

23. Tisserand F. *Traité de Mechanique Céleste, Tome II*. Paris: Gauthier–Villars; 1889.

24. Zotos EE. Trapped and escaping orbits in an axially symmetric galactic–type potential. *PASA*. 2012;29:161-173.

25. Zotos EE. Escape dynamics in a Hamiltonian system with four exit channels. *Nonlinear Studies*. 2015;22(3):1-20.

26. Zotos EE. Escape and collision dynamics in the planar equilateral restricted four-body problem. *International Journal of Non-Linear Mechanics* 2016;86:66-82.

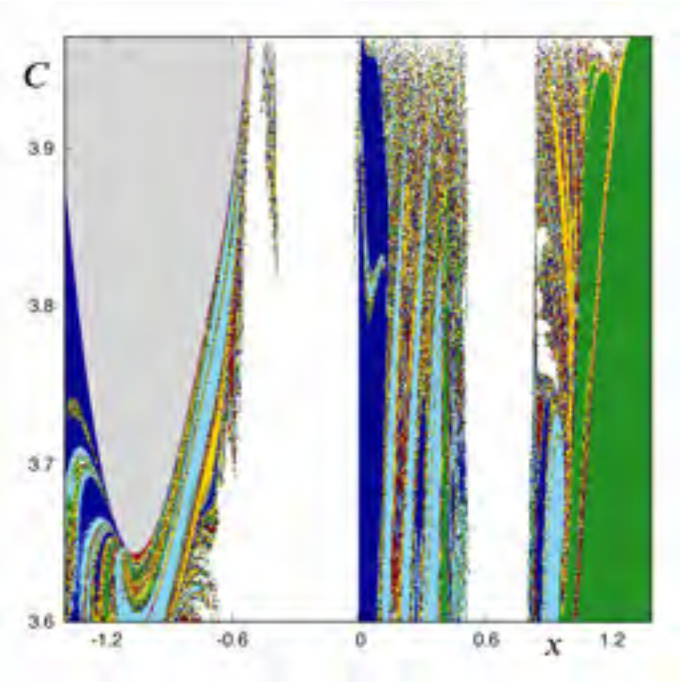

FIGURE 13 Structure of the plane (x, C) for $N = 5$, and a maximum time of integration of $T = 10^2$.